RAPID COMMUNICATION

Strontium optical lattice clock at the National Time Service Center*

Ye-Bing Wang(王叶兵)[1,2], Mo-Juan Yin(尹默娟)[1], Jie Ren(任洁)[1], Qin-Fang Xu(徐琴芳)[1], Ben-Quan Lu(卢本全)[1,2], Jian-Xin Han(韩建新)[1,2], Yang Guo(郭阳)[1,2], and Hong Chang(常宏)[1,†]

[1] *CAS Key Laboratory of Time and Frequency Primary Standards, National Time Service Center, Xi'an* 710600, *China*

[2] *University of Chinese Academy of Sciences (CAS), Beijing* 100049, *China*

(Received 1 December 2017; revised manuscript received 18 December 2017; published online 29 January 2018)

We report the ^{87}Sr optical lattice clock developed at the National Time Service Center. We achieved a closed-loop operation of the optical lattice clock based on ^{87}Sr atoms. The linewidth of the spin-polarized clock peak is 3.9 Hz with a clock laser pulse length of 300 ms, which corresponds to a Fourier-limited linewidth of 3 Hz. The fitting of the in-loop error signal data shows that the instability is approximately $5\times10^{-15}\tau^{-1/2}$, affected primarily by the white noise. The fractional frequency difference averages down to 5.7×10^{-17} for an averaging time of 3000 s.

Keywords: optical clock, optical lattice, strontium atoms, stability

PACS: 37.10.Jk, 32.70.Jz, 06.30.Ft, 42.62.Eh **DOI:** 10.1088/1674-1056/27/2/023701

1. Introduction

Over the past decade, the progress in optical clocks has been of key importance for the advancement of science and technology. Optical clocks can be used in the field of scientific research, such as fundamental constants variation measurement,[1–3] gravitational wave detection,[4] topological dark matter hunting,[5] and space research and applications.[6] In addition, optical clocks have been investigated for global navigation satellite systems and geodetic applications.[7]

The fractional frequency instability and uncertainty of the best optical clocks based on neutral atoms[8–11] and single ions[7,12,13] have reached the unprecedented level of 10^{-18}, which can be employed to redefine the unit of second of the international system of units (SI) using optical clocks. Owing to the smallest fractional frequency instability and uncertainty as well as promising results from the extensive research, ^{87}Sr optical lattice clock is one of the most promising candidates for the redefinition of the unit of second. The first optical lattice clock based on ^{87}Sr has been developed at the University of Tokyo.[14] ^{87}Sr optical lattice clocks have also been demonstrated at the National Metrology Institute of Japan (NMIJ), Physikalisch-Technische Bundesanstalt (PTB), Sytèmes de Référence Temps Espace (SYRTE), and the National Institute of Information and Communications Technology (NICT) in Japan. Recently, a research team of the Joint Institute for Laboratory Astrophysics (JILA) obtained a measurement precision of 5×10^{-19} in an averaging time of 1 h based on a ^{87}Sr optical lattice clock,[15] which benefits from the high correlated density of the degenerate Fermi gas in the three-dimensional (3D) optical lattice to prevent on-site interaction shifts.

The first optical clock in China was constructed at the Wuhan Institute of Physics and Mathematics (WIPM) of the Chinese Academy of Sciences which was based on the single $^{40}Ca^{+}$-ion,[16–18] while the first ^{87}Sr optical lattice clock in China was constructed at the National Institute of Metrology (NIM).[19] This was followed by the development of various types of optical clocks based on atoms of Yb[20–22] and Hg,[23,24] ions of Hg^{+}[25] and Al^{+},[26,27] etc. Based on the observation of the $(5s^2)^1S_0$–$(5s5p)^3P_0$ transition spectrum of bosonic ^{88}Sr,[28] we began to develop an optical lattice clock based on the fermionic ^{87}Sr from August 2016. After approximately one year of development, we achieved the closed-loop operation of the ^{87}Sr optical lattice clock. A fractional frequency instability of 5.7×10^{-17} was obtained for an averaging time of 3000 s. In this paper, we describe in details the setup of our strontium optical lattice clock, which can be beneficial for future optical-clock experiments.

2. Principle of operation of the ^{87}Sr optical lattice clock

The energy levels and transitions of ^{87}Sr used for the development of the optical lattice clock are illustrated in Fig. 1. The ^{87}Sr atoms are three-dimensional magneto-optical trapped (MOT) with the transition of $(5s^2)^1S_0(F=9/2)$–$(5s5p)^1P_1(F=11/2)$ which corresponds to a wave-

*Project supported by the National Natural Science Foundation of China (Grant Nos. 11474282 and 61775220), the Key Research Project of Frontier Science of the Chinese Academy of Sciences (Grant No. QYZDB-SSW-JSC004), and the Strategic Priority Research Program of the Chinese Academy of Sciences (Grant No. XDB21030700).

†Corresponding author. E-mail: changhong@ntsc.ac.cn

length of 461 nm. The natural linewidth of this transition is 32 MHz, leading to a cooling limit temperature at the millikelvin level. Lasers with wavelengths of 679 nm and 707 nm are used to repump the atoms in the levels of $(5s5p)^3P_2$ and $(5s5p)^3P_0$ to $(5s5p)^3P_1$ through the $(5s5p)^3P_0$–$(5s6s)^3S_1$ and $(5s5p)^3P_2$–$(5s6s)^3S_1$ transitions, which eventually decay to the ground state. The ^{87}Sr atoms are further cooled and trapped though the intercombination transition of $(5s^2)^1S_0(F = 9/2)$–$(5s5p)^3P_1(F = 11/2)$ at 689 nm. The Doppler limit is in the sub-microkelvin range owing to the narrow linewidth of 7.5 kHz. In order to increase the efficiency of the laser cooling, another laser called stirring laser which is slightly red-detuned from the transition of $(5s^2)^1S_0(F = 9/2)$–$(5s5p)^3P_1(F = 9/2)$ at 689 nm is used to provide population randomization among the different spin states. In addition, this laser is also used as the pump laser in the stage of state preparation to ensure pure polarization. The 813-nm lattice laser provides a clock-transition immunity against recoil and AC Stark shifts. The transition of $(5s^2)^1S_0(F = 9/2)$–$(5s5p)^3P_0(F = 9/2)$ is the clock transition with a neutral linewidth of approximately 1 mHz owing to the hyperfine interaction effects. The absolute transition frequency of the clock is 429228004229873 Hz, hence the Q-value of the ^{87}Sr optical lattice clock is approximately 4×10^{17}. After the interrogation by a 698-nm clock laser pulse, the excitation fraction is detected by monitoring the florescence excited by the 461-nm laser.

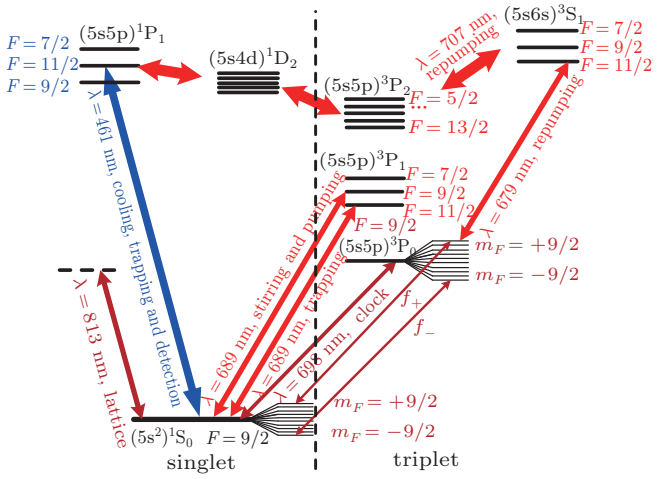

Fig. 1. (color online) Energy-levels schematic of a ^{87}Sr atom.

3. Experimental setup

A top view of the experimental setup of the ^{87}Sr optical lattice clock is shown in Fig. 2. The strontium atomic beam effuses from an oven heated to a temperature of 500 °C. The velocity of the atomic beam is decreased from approximately 460 m/s to 50 m/s by a Zeeman slower with ten coils. In general, there are 30 laser beams at different wavelengths propagating in the setup. Three trapping laser beams and their corresponding reflection beams at 461 nm are used to form a blue MOT with a magnetic field produced by two anti-Helmholtz coils. The laser beams at 679 nm and 707 nm are used to increase the number of atoms in the blue MOT. The three trapping laser beams at 689 nm are overlapped with the 461-nm trapping laser beams to form a red MOT. The 813-nm laser beam and reflected beam are focused on the atom cloud to form a one-dimensional (1D) lattice, in order to load atoms for the clock interrogation. A photomultiplier tube (PMT) is used to detect the fluorescence signals of the 461-nm probe laser. The temperature of the atoms in the MOT is measured with an electron multiplying charge-coupled device (EMCCD) using the time-of-flight (TOF) method.

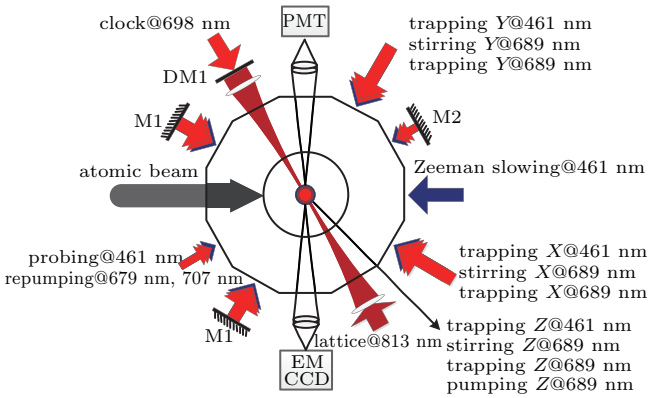

Fig. 2. (color online) Top view of the experimental setup. M1: 0°-high-reflection mirror at 461 nm and 689 nm; M2: 0°-high-reflection mirror at 461 nm, 679 nm, and 707 nm; DM1: 0°-dichroic mirror with a high reflection at 813 nm and high transmittance at 698 nm.

3.1. First stage of cooling and trapping

The experimental setup of the first stage of cooling and trapping is shown in Fig. 3. The 461-nm laser produced through a second-harmonic generation from a 922-nm external cavity diode laser (ECDL) is locked to the $(5s^2)^1S_0$–$(5s5p)^1P_1$ transition of the ^{88}Sr atomic beam, owing to the largest natural abundance of 82.56%, and exhibits a detuning of 51.8 MHz from the $(5s^2)^1S_0(F = 9/2)$–$(5s5p)^1P_1(F = 11/2)$ transition of ^{87}Sr. The locked laser is used to produce the Zeeman slowing laser, trapping laser and atomic-states probe laser with detuning values of −560 MHz, −40 MHz, and 0 MHz, respectively, by acousto-optic modulators (AOMs); their output powers are 50 mW, 40 mW, and 1 mW, respectively. The ^{87}Sr atoms from the strontium thermal atomic beam are cooled using the Zeeman slower and trapped in the blue MOT with an axial magneticfield gradient of 50 Gs/cm (1 Gs = 10^{-4} T).

The laser frequency of the 707-nm ECDL with a mode spacing of approximately 5 GHz is scanned using a frequency of 1 kHz through the current control and piezoelectric transducer (PZT), in order to cover all hyperfine transitions. The

frequency scanning range can be measured by the Cavity 1. The laser beams at 679 nm (ECDL) and 707 nm are coupled to an optical fiber for a spatial filtering, and used to repump atoms for the cooling cycle in the first stage of cooling and trapping. These laser beams have powers of 8 mW (679 nm) and 10 mW (707 nm), respectively. The number of atoms can increase approximately 15 times. After the first stage of cooling and trapping, the temperature and number of atoms in the blue MOT are 5 mK and 2.3×10^7, respectively.

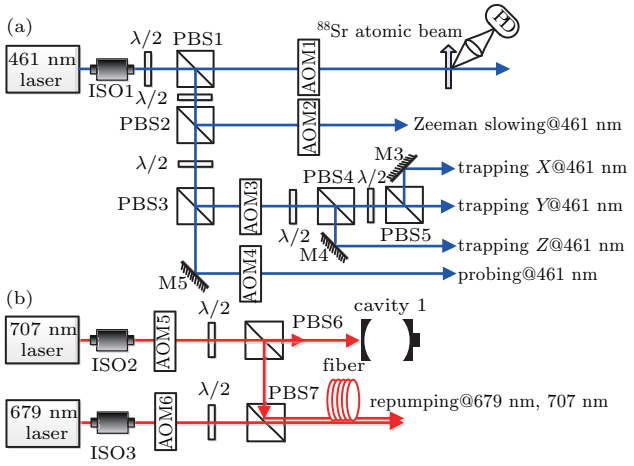

Fig. 3. (color online) Laser sources for the first stage of cooling and trapping. (a) Laser source at 461 nm. (b) Laser sources at 679 nm and 707 nm. ISO1–3: optical isolators at 461 nm, 707 nm, and 679 nm, respectively; PD: photodiode; PBS1–5: polarizing beam splitters at 461 nm; PBS6–7: polarizing beam splitters at 707 nm and 679 nm, respectively; $\lambda/2$: half-wave plate; $\lambda/4$: quarter-wave plate; M3–5: 45°-high-reflection mirrors at 461 nm; AOM1–4: acousto-optic modulators at 461 nm with frequency shifts of +312 MHz, −300 MHz, +220 MHz, and +260 MHz, respectively; AOM5 and AOM6 are acousto-optic modulators at 707 nm and 679 nm, respectively, with frequency shifts of +80 MHz.

3.2. Second stage of cooling and trapping

The experimental setup of the second stage of cooling and trapping is shown in Fig. 4. The 689-nm ECDL is locked to an ultra-low-expansion (ULE) cavity with a fineness of approximately 10000 at 689 nm using the Pound–Drever–Hall (PDH) technique. It is used to produce the second stage cooling and trapping laser, stirring laser, and pumping laser. The linewidth of the 689-nm laser is approximately 300 Hz, which is suitable for a narrow-line cooling; its power is approximately 8 mW. In order to increase the power of the 689-nm beam, two slave diode lasers are injection-locked to the master laser; one of them as a cooling and trapping laser, while the other one as stirring and pumping lasers. The laser power for cooling and trapping is approximately 7 mW, while those for stirring and pumping are 3 mW and 0.2 mW, respectively. The typical transfer efficiency of atoms from the blue MOT to the red MOT is approximately 15%. The temperature and number of atoms in the red MOT are 3.9 μK and 3.5×10^6, respectively. The pump laser is used before the clock interrogation in order to pump atoms from ten Zeeman levels to either stretched states of $m_F = \pm 9/2$; the rotation direction of the pump beam is switched between the σ^+ and σ^- polarizations by a liquid-crystal variable wave-plate.

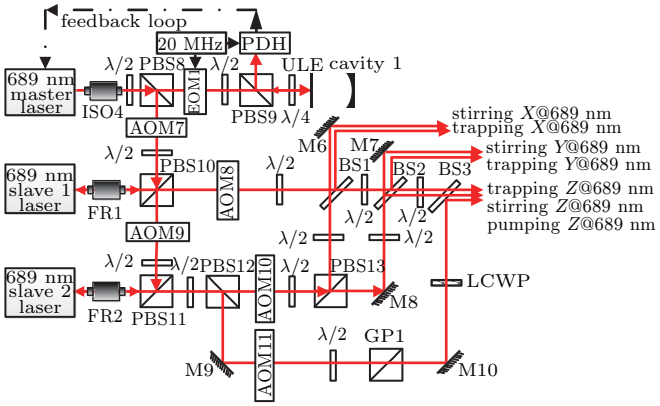

Fig. 4. (color online) Laser sources for the second stage of cooling and trapping. ISO4: optical isolators at 689 nm; FR1–2: Faraday Rotators at 689 nm; BS1–3: beam splitters with ratios between reflection and transmission of 3:7, 5:5, and 1:9, respectively; PBS8–13: polarizing beam splitters at 689 nm; $\lambda/2$: half-wave plate; $\lambda/4$: quarter-wave plate; M6–10: 45°-high-reflection mirrors at 689 nm; EOM1: electro-optic modulator; AOM7–11: acousto-optic modulators at 689 nm with frequency shifts of +100 MHz, −244 MHz, +1026 MHz, +195 MHz, and +195 MHz, respectively; GP1: Glan prism; LCWP: liquid-crystal wave-plate.

3.3. Lattice loading and clock transition probing

The experimental setups of the lattice loading and clock transition probing are shown in Fig. 5. Approximately 10^4 atoms are loaded into a 1D optical lattice at a magic wavelength of 813 nm. The frequency of the 813-nm laser is locked to the low-fineness ($F = 200$) Cavity 2. The $1/e$ waist diameter of the 813-nm laser is designed to be approximately 120 μm, while its power is 300 mW, indicating a trap lattice

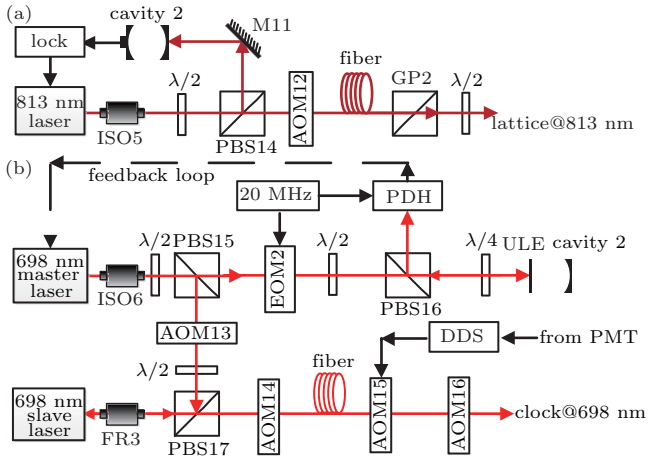

Fig. 5. (color online) Laser sources for lattice loading and clock-transition probing. (a) Source for the 813-nm lattice laser. (b) Source for the 698-nm clock laser. ISO5 and ISO6: optical isolators at 813 nm and 698 nm, respectively; FR3: Faraday Rotators at 698 nm; PMT: photomultiplier tube; DDS: direct digital synthesizer; PBS14 and PBS15–17: polarizing beam splitters at 813 nm and 698 nm, respectively; $\lambda/2$: half-wave plate; $\lambda/4$: quarter-wave plate; M11: 45°-high-reflection mirror at 813 nm; EOM2: electro-optic modulator; AOM12: acousto-optic modulator at 813 nm with a frequency shift of −200 MHz; AOM13–16: acousto-optic modulators at 698 nm with frequency shifts of −220 MHz, −80 MHz, −199 MHz, and −208 MHz, respectively; GP2: Glan prism.

depth of approximately $56E_r$, where E_r is the lattice-photon recoil energy. The 698-nm laser is locked to a ULE Cavity 2 whose fineness is approximately 4×10^5 using the PDH technique. Therefore, the linewidth of the 698-nm laser is approximately 1 Hz. The 698-nm laser is directed to the atoms with a 5-m optical fiber using a fiber phase-noise cancellation system. The frequency of the clock laser is tuned by an AOM15, which provides a scanning across the resonance frequency of the ^{87}Sr-clock transition. The waist of the 698-nm clock beam is approximately 600 μm, which is suitable for homogeneously exciting the atoms;[29] its power is approximately 100 nW.

3.4. Timing sequence

The timing sequence in the ^{87}Sr optical lattice clock experiment is shown in Fig. 6. Once the blue MOT switched off, the axial magnetic-field gradient is decreased from 50 Gs/cm to 3 Gs/cm in 1 ms. The magnetic field gradient of 3 Gs/cm is maintained for 10 ms, and then it is increased to 10 Gs/cm slowly during a period of 90 ms in order to compress the cloud of cold atoms. In order to decrease the atomic temperature, the 689-nm laser is set to a single-frequency mode. During the second cooling, the atoms with a temperature below the lattice-depth temperature are trapped in the optical lattice formed by the 813-nm laser. The atoms in all m_F states will be set to the $(5s^2)^1S_0(m_F = +9/2)$ or $(5s^2)^1S_0(m_F = -9/2)$ states using the polarized pump laser at 689 nm. The clock is interrogated using the 698-nm clock laser and probed with the 461-nm laser. In order to increase the signal-to-noise ratio and decrease the effect of the fluctuation of the atomic number in each cycle, a normalized shelving detection scheme is used. With four cycles, the error signal can be calculated from the excitation fraction of the two stretched states.

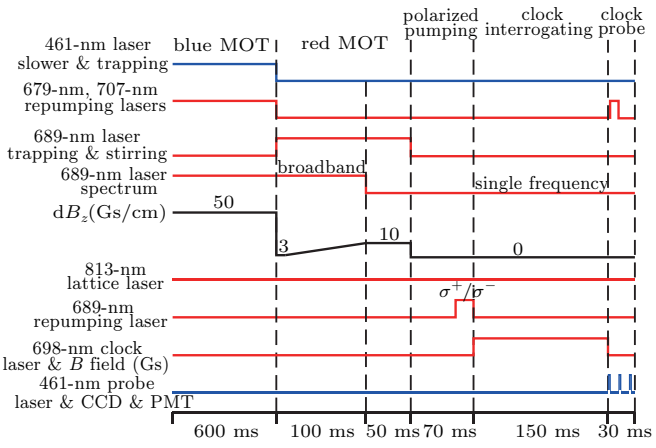

Fig. 6. (color online) Timing scheme in the ^{87}Sr optical lattice clock experiment.

4. Recent experimental result

4.1. Lifetime of atoms in the lattice

The number of atoms trapped in the lattice can be measured through the fluorescence intensity of the atomic cloud in the optical lattice using the PMT. The fluorescence intensity as a function of the holding time is recorded and shown in Fig. 7. The black points represent the experimental data, while the curve represent the exponential-decay fitting function. The fitting shows that the $1/e$ lifetime is approximately 1.6 s, mainly affected by the background-gas collisions, Sr-atoms collisions, and intensity noise of the 813-nm lattice laser. For the optical lattice clock, for a longer lifetime of the atoms trapped in the lattice, a longer interrogation time can be used.

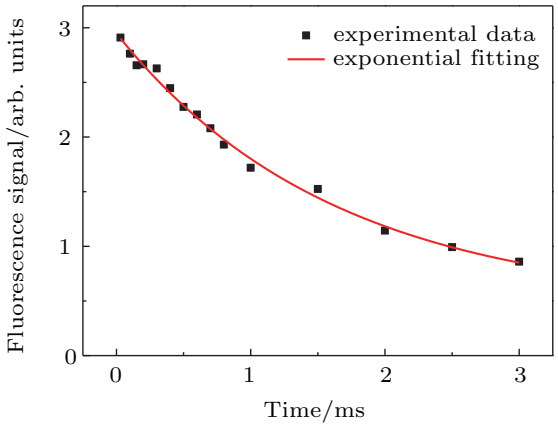

Fig. 7. (color online) Lifetime of the atoms trapped in the 1D optical lattice.

4.2. Clock transition spectra of ^{87}Sr

4.2.1. Resolved sideband spectroscopy and high-resolution carrier spectroscopy of the clock transition

Resolved sideband spectroscopy of the ^{87}Sr $(5s^2)^1S_0$–$(5s5p)^3P_0$ transition is performed and shown in Fig. 8, by scanning the frequency of the clock laser though AOM15 using the normalized detection method.[30] It consists of a narrow carrier peak in the center, red sideband and blue sideband. The pulse length of the clock laser is 150 ms with a Fourier-limited Rabi linewidth of 6 Hz. The full width at half maximum of the resolved sideband spectra is 455 Hz mainly owing to the power broadening; a scan step of 200 Hz and scan range larger than 160 kHz were employed. The power of the 698-nm clock laser is 400 μW, while the beam waist is 120 μm. The trap frequency along the longitudinal direction is approximately 75 kHz; the longitudinal temperature of the atoms can be estimated from the relative heights of the blue and red sidebands. The spectra in Fig. 8 reveals that the temperature along the longitudinal direction is approximately 4.2 μK.

The inset of Fig. 8 shows high-resolution carrier spectroscopy results of the clock transition observed with a pulse

length of the clock laser of 150 ms and scan step of 2 Hz. The black points represent the experimental data, while the red curve represents the Lorentzian fitting function. The linewidth of the spectrum is 6.7 Hz, very close to the Fourier-limited Rabi linewidth of 6 Hz.

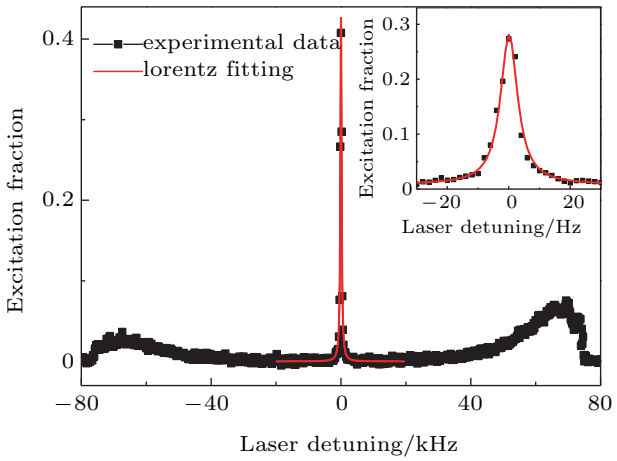

Fig. 8. (color online) Resolved sideband spectroscopy of the ^{87}Sr clock transition. High-resolution carrier spectroscopy of the clock transition is shown in the inset.

4.2.2. Resolved Zeeman spectra and spin-polarized spectra

With a small bias magnetic field along the polarization axis of the clock and lattice lasers, ten separated distinct π-polarized Zeeman transitions[31] from the individual m_F states are shown in Fig. 9. The labels shown in the figure correspond to the transitions from the ground sublevel states; the intensities of the individual π-polarized transitions are determined using the Clebsch–Gordan coefficients.

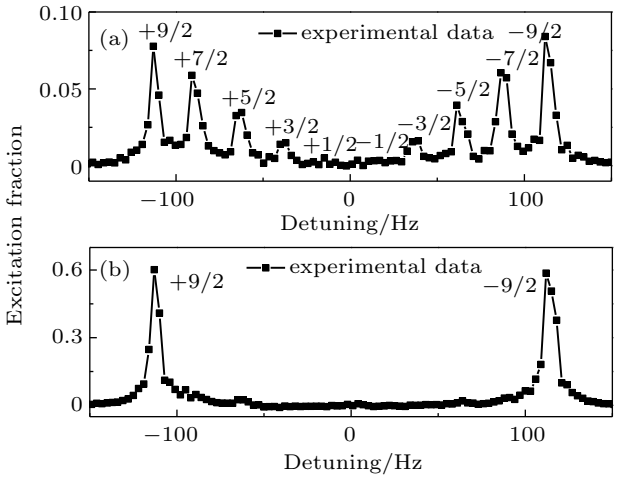

Fig. 9. (a) Resolved Zeeman spectrum of the π transitions. (b) Spin-polarized spectra of the transitions from $m_F = +9/2$ to $m_F = +9/2$ and from $m_F = -9/2$ to $m_F = -9/2$.

In order to increase the signal-to-noise ratio and excitation fraction, we pump the atoms into either stretched states of $m_F = \pm 9/2$ at the ground state using a weak 689-nm laser resonant with the $(5s^2)^1S_0(F = 9/2)$–$(5s5p)^3P_1(F = 9/2)$ transition. The pump-laser beam propagates along the vertical direction perpendicular to the direction of the lattice and clock lasers. With a σ^+ or σ^- polarized 689-nm laser, the atoms in all m_F states will be prepared in the $(5s^2)^1S_0(m_F = +9/2)$ or $(5s^2)^1S_0(m_F = -9/2)$ states, respectively. More than 90% of the atoms are pumped to either of the two stretched states; the excitation fraction is approximately 7 times more than that achieved without a pumping laser.

For the pulse length of the clock laser of 300 ms, the linewidth of both peaks is 3.9 Hz, obtained by the Lorentzian fit of the data, which corresponds to a Fourier-limited linewidth of 3 Hz.

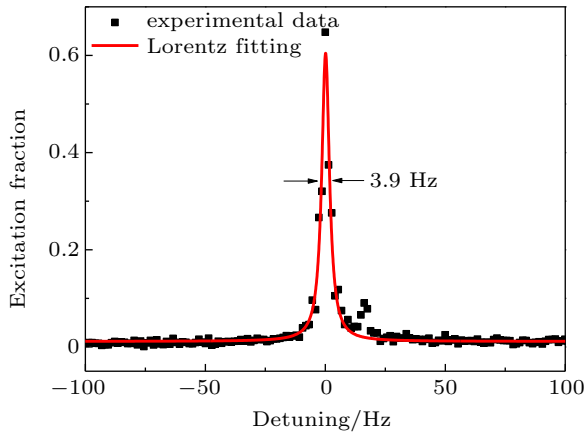

Fig. 10. (color online) Spin-polarized spectra of the transition from $m_F = +9/2$ to $m_F = +9/2$.

4.3. Closed-loop operation of the ^{87}Sr optical lattice clock

Using the spin-polarized spectra of $m_F = +9/2$–$m_F = +9/2$ and $m_F = -9/2$–$m_F = -9/2$ Zeeman transitions as the reference of frequency, the first-order Zeeman shift and vector Stark shift can be canceled.[19] Using the differences of the excitation fractions at the half maximum points of each spin-polarized spectrum in Fig. 9(b), the error signal can be calculated and the frequency of the clock laser can be locked to the clock transition of the ^{87}Sr atom using the AOM15. The probe period is 1 s, while the feedback cycle of the clock is 4 s. The optical lattice clock can run continuously for more than 5 h.

Using the error signal from the clock laser locking to the clock transition, we can evaluate the in-loop instability of the ^{87}Sr optical lattice clock by calculating the Allan deviation.[20] The in-loop fractional frequency instability is 5.7×10^{-17} at an averaging time of 3000 s, which represents the best level for our interleaved measurement (Fig. 11). The fitting shows that the instability is $5 \times 10^{-15}/\tau^{1/2}$, affected mainly by the white noise.

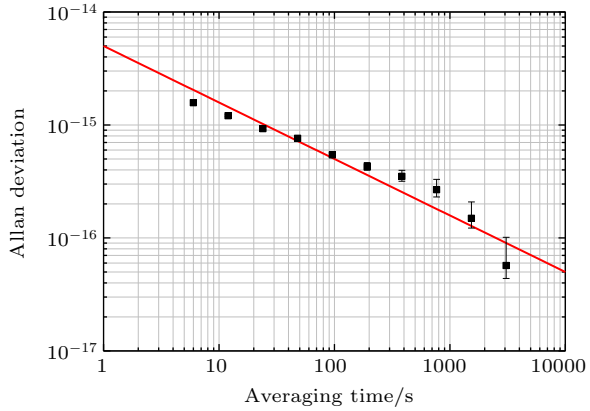

Fig. 11. (color online) In-loop fractional frequency instability of the ^{87}Sr optical lattice clock.

5. Conclusion and perspectives

We achieved a closed-loop operation of an optical lattice clock based on ^{87}Sr atoms for more than 5 h. The linewidth of the spin-polarized spectra was 3.9 Hz with a pulse length of the clock laser of 300 ms, which corresponds to a Fourier-limited linewidth of 3 Hz. The fitting of the in-loop error signal data shows that the instability is $5 \times 10^{-15}/\tau^{1/2}$, affected mainly by the white noise. The fractional frequency difference averages down to 5.7×10^{-17} at an averaging time of 3000 s. The described setup and key technologies could be of benefit for future optical-clock experiments. The instability of the ^{87}Sr optical lattice clock may be further improved experimentally, which would be very important for science and technology.

References

[1] Blatt S, Ludlow A D, Campbell G K, Thomsen J W, Zelevinsky T, Boyd M M, Ye J, Baillard X, Fouché M, Le Targat R, Brusch A, Lemonde P, Takamoto M, Hong F L, Katori H and Flambaum V V 2008 *Phys. Rev. Lett.* **100** 140801

[2] Godun R M, Nisbet-Jones P B R, Jones J M, King S A, Johnson L A M, Margolis H S, Szymaniec K, Lea S N, Bongs K and Gill P 2014 *Phys. Rev. Lett.* **113** 210801

[3] Huntemann N, Lipphardt B, Tamm Chr, Gerginov V, Weyers S and Peik E 2014 *Phys. Rev. Lett.* **113** 210802

[4] Kolkowitz S, Pikovski I, Langellier N, Lukin M D, Walsworth R L and Ye J 2016 *Phys. Rev. D* **94** 124043

[5] Derevianko A and Pospelov M 2014 *Nat. Phys.* **10** 933

[6] Ludlow A D, Boyd M M, Ye J, Peik E and Schmidt P O 2015 *Rev. Mod. Phys.* **87** 637

[7] Chou C W, Hume D B, Rosenband T and Wineland D J 2010 *Science* **329** 1630

[8] Bloom B J, Nicholson T L, Williams J R, Campbell S L, Bishof M, Zhang X, Zhang W, Bromley S L and Ye J 2014 *Nature* **506** 71

[9] Hinkley N, Sherman J A, Phillips N B, Schioppo M, Lemke N D, Beloy K, Pizzocaro M, Oates C W and Ludlow A D 2013 *Science* **341** 1215

[10] Nicholson T L, Campbell S L, Hutson R B, Marti G E, Bloom B J, McNally R L, Zhang W, Barrett M D, Safronova M S, Strouse G F, Tew W L and Ye J 2015 *Nat. Commun.* **6** 6896

[11] Ushijima I, Takamoto M, Das M, Ohkubo T and Katori H 2015 *Nat. Photon.* **9** 185

[12] Huntemann N, Sanner C, Lipphardt B, Tamm Chr and Peik E 2016 *Phys. Rev. Lett.* **116** 063001

[13] Chou C W, Hume D B, Koelemeij J C J, Wineland D J and Rosenband T 2010 *Phys. Rev. Lett.* **104** 070802

[14] Takamoto M, Hong F L, Higashi R and Katori H 2005 *Nature* **435** 321

[15] Campbell S L, Hutson R B, Marti G E, Goban A, Darkwah Oppong N, McNally R L, Sonderhouse L, Robinson J M, Zhang W, Bloom B J and Ye J 2017 *Science* **358** 90

[16] Huang Y, Cao J, Liu P, Liang K, Ou B, Guan H, Huang X, Li T and Gao K 2012 *Phys. Rev. A* **85** 030503

[17] Huang Y, Guan H, Liu P, Bian W, Ma L, Liang K, Li T and Gao K 2016 *Phys. Rev. Lett.* **116** 013001

[18] Huang Y, Liu Q, Cao J, Ou B, Liu P, Guan H, Huang X and Gao K 2011 *Phys. Rev. A* **84** 053841

[19] Lin Y G, Wang Q, Li Y, Meng F, Lin B K, Zang E J, Sun Z, Fang F, Li T C and Fang Z J 2015 *Chin. Phys. Lett.* **32** 090601

[20] Liu H, Zhang X, Jiang K L, Wang J Q, Zhu Q, Xiong Z X, He L X and Lyu B L 2017 *Chin. Phys. Lett.* **34** 020601

[21] Zhou M and Xu X Y 2016 *AAPPS Bulletin* **26** 10

[22] Xu Y L and Xu X Y 2016 *Chin. Phys. B* **25** 103202

[23] Liu K K, Zhao R C, Gou W, Fu X H, Liu H L, Yin S Q, Sun J F, Xu Z and Wang Y Z 2016 *Chin. Phys. Lett.* **33** 070602

[24] Liu H L, Yin S Q, Liu K K, Qian J, Xu Z, Hong T and Wang Y Z 2013 *Chin. Phys. B* **22** 043701

[25] Liu J P, Li J G and Zou H X 2017 *Chin. Phys. B* **26** 023104

[26] Shang J J, Cui K F, Cao J, Wang S M, Chao S J, Shu H L and Huang X R 2016 *Chin. Phys. Lett.* **33** 103701

[27] Zhang J, Deng K, Luo J and Lu Z H 2017 *Chin. Phys. Lett.* **34** 050601

[28] Xu Q F, Liu H, Lu B Q, Wang Y B, Yin M J, Kong D H, Ren J, Tian X and Chang H 2015 *Chin. Opt. Lett.* **13** 100201

[29] Blatt S, Thomsen J W, Campbell G K, Ludlow A D, Swallows M D, Martin M J, Boyd M M and Ye J 2009 *Phys. Rev. A* **80** 052703

[30] Zhang M J, Liu H, Zhang X, Jiang K L, Xiong Z X, Lü B L and He L X 2016 *Chin. Phys. Lett.* **33** 070601

[31] Wang Q, Lin Y G, Li Y, Lin B K, Meng F, Zang E J, Li T C and Fang Z J 2014 *Chin. Phys. Lett.* **31** 123201